DOI: 10.1002/ejic.200801208

# Synthesis and Characterization of a Series of New Luminescent NHC-Coordinated $Au^I$–$Ag^I$ Tetra- and Polymetallic Complexes Containing Benzoate-Bridged $Ag_2$ Dimers

**Amit K. Ghosh[a] and Vincent J. Catalano*[a]**

**Keywords:** Gold / Silver / Aurophilicity / N-Heterocyclic carbenes / Coordination polymers

The reaction of $[Au(CH_3impy)_2]PF_6$ (**2**), with substituted silver benzoate salts bearing different halide substituents produced a series of new mixed-metal species having two different structural motifs. One structural motif contains discrete tetrametallic $Ag_2Au_2$ diamond cores, whereas the other motif contains the same tetrametallic diamond core interconnected by benzoate-bridged silver dimers to form polymers. All the complexes are substitution-inert and stable both in the solid state as well as in solution. We also report the synthesis of oxidative addition products of $[Au(CH_3impy)_2]PF_6$, which were also obtained during our attempts to oxidize the above-mentioned multimetallic assembly with bromine and iodine. Compounds **3**–**7** are intensely luminescent in frozen acetonitrile solution, but surprisingly no luminescence is observed at room temperature. All the complexes were completely characterized by $^1H$, $^{13}C$ NMR, electronic absorption, emission spectroscopy, elemental analysis and X-ray crystallography.



## Introduction

It is well established[1–3] that closed-shell, $d^{10}$ metal ions often exhibit attractive interactions. These interactions, although weaker than ionic bonds, are stronger than simple van der Waals interactions. The most prominent of these metallophilic interactions are the so-called aurophilic attractions[4–6] found between $d^{10}$ $Au^I$ centers. To a lesser extent the argento–aurophilic interactions found between mixed $d^{10}$ $Ag^I$–$Au^I$ centers are also proving to be interesting.[7,8] Several theoretical studies[9] have addressed the nature of these interactions with most studies leading to dispersion forces and relativistic effects as the primary attractive forces. The role of dispersion forces[10] in metallophilic interactions became clear only about five years ago, whereas the role of relativistic effects[11,4] have been long understood. The theoretical chemistry of gold was thoroughly reviewed by Pyykkö[12] who elegantly describes aurophilicity simply as an usually strong van der Waals attraction in an unusual place. In case of mixed-metal interactions, introduction of dissimilar metals induces enhanced dispersion forces due to an increase in dipolar interactions, which in turn results in smaller metal–metal separation than for homometallic systems.[13,14]

Recently, we have focused our attention on various N-heterocyclic carbene (NHC) ligands which, through their strong σ donation, very reliably hold metal centers in suitable juxtaposition in order to study such $d^{10}$–$d^{10}$ interactions.[15] One such species is derived from the precursor 1-methyl-3-(2-pyridinyl)-1*H*-imidazolium hexafluorophosphate, $[H(CH_3impy)]PF_6$. It was observed[15b] (Scheme 1) before that the Au complex of this ligand, when treated with $AgBF_4$ in presence of a nitrile solvent such as $CH_3CN$, produced polymeric species $\{[AuAg(CH_3impy)_2(S)](BF_4)_2\}_n$, where S stands for solvent. In these mixed-metal, one-dimensional polymers, the $Au^I$ centers are bonded to two carbene moieties, and the $Ag^I$ centers are coordinated to two alternating pyridyl groups and a solvent molecule. The solid-state structures of these polymers are greatly influenced by the steric and electronic properties of the auxiliary ligands. For example, simply changing the coordinated nitrile from acetonitrile to benzonitrile to benzylnitrile, greatly alters the geometry about the multimetallic polymeric backbone. In the acetonitrile polymer, the $d^{10}$–$d^{10}$ metal–metal separations between the alternating $Au^I$ and $Ag^I$ centers are small and range from 2.8633(6) to 2.9239(6) Å. The intermetallic angles deviate significantly from linearity and range from 135.20(2) to 175.37(3)°. Replacement of the acetonitrile solvent with benzonitrile produces a similar type of polymer, but the metal–metal separations are much more uniform and range from 2.833(1) to 2.835(1) Å. Similarly, the intermetallic angles are also more regular at 162.429(8) and 179.86(4)°. The benzylnitrile-containing polymer was very similar to the benzonitrile counterpart. The only difference is that the metal–metal separations were slightly enlarged [2.8448(5) and 2.8940(5) Å]. The zig-zag polymeric chain in this polymer has two different intermetallic angles of 148.919(9) and 170.87(2)°, respectively. Replacement of

[a] Department of Chemistry, University of Nevada, Reno, NV 89557, USA
Fax: +1-775-784-6804
E-mail: vjc@unr.edu

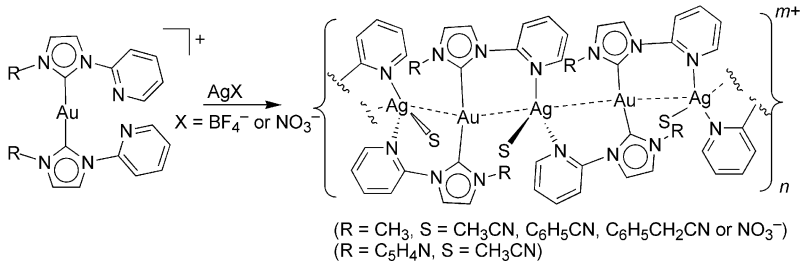


Scheme 1.

the coordinated nitrile with a nitrate anion produced a fourth polymer with distinct intermetallic angles and distances. The intermetallic separation in this material ranges from 2.8125(2) to 2.9428(2) Å, and the intermetallic angles are more acute [131.321(8) and 140.915(7)°] than those of the other polymers described above.

Substitution of the auxiliary groups on the imidazole ligand also profoundly changes the polymeric structure. For example, the bis(pyridyl)-substituted imidazole NHC ligand readily forms (Scheme 1) an $Ag^I$–$Au^I$ helical polymer.[16] Interestingly, this material crystallizes in a chiral fashion with a statistical mixture of both the left-handed and right-handed crystals. Apart from the differences in helicity, the two enantiomers are completely identical with relatively small intermetallic separations of 2.8359(4) and 2.9042(4) Å. The angles around each Ag atom are slightly bent at 171.804(12) and 166.176(13)°, respectively.

In an attempt to study the electronic influences of the auxiliary ligands, we set out to prepare a series of complexes with similar steric profiles, but with easily tunable electronic factors. Herein, we report the reaction of $[Au(CH_3impy)_2]PF_6$ (**2**), with unsubstituted as well as *ortho*- and *para*-substituted silver benzoates bearing different halides. To our surprise, a completely different set of complexes with an entirely different structural motif is observed.

## Results

As shown in Scheme 2, the Au complex, $[Au(CH_3impy)_2]PF_6$ (**2**), obtained by a simplified procedure, was treated with silver benzoate and four other substituted silver benzoates generating two distinct structural motifs. In the case of silver benzoate and silver 4-fluorobenzoate, polymeric 1-dimensional assemblies, **3** and **4**, were obtained whereas in case of silver 4-chlorobenzoate, silver 2,4-dichlorobenzoate and silver 4-bromobenzoate, discrete tetrametallic complexes **5**–**7** were formed. As shown in Scheme 2, each complex contains a tetrametallic $Ag_2Au_2$ unit in its core. In the first class (complexes **3** and **4**) these cores are strongly interconnected by a dimetallic, benzoate-bridged $Ag_2$ dimer, whereas in the second class (**5**–**7**) discrete tetrametallic cores are isolated. In each tetrametallic assembly the $Au^I$ centers are linearly coordinated to two NHC ligands whose pendant pyridyl group coordinates to an adjacent $Ag^I$ center. Additionally, these Ag centers are bridged in a *trans* fashion by two benzoate anions. In polymers **3** and **4**, the linking $[Ag(benzoate)]_2$ dimers are additionally coordinated to two acetonitrile molecules.

Notably, all the reactions were initially carried out by using the same stoichiometry (1:2.5) of Au complex **2**/silver benzoate. However, the Au/Ag ratio in the products varies from 1:1 in the tetrametallic assembly to 1:2 in the polymeric species. Addition of silver benzoates to complexes **5**–**7** does not produce the respective polymeric species, nor could any mixed benzoate polymers be isolated. Lowering of the ratio to 1:1 in the synthesis of **3** and **4** only reduces the overall yield, and the same products were isolated. Interestingly, when the benzoate rings contain strong electronegative substituents (**4** and **6**), the products were obtained at room temperature, whereas in other cases the reaction mixtures had to be refluxed. All of these products were reproducibly obtained.

Attempts to oxidize the polymeric complexes or the tetrametallic assemblies with bromine or iodine fragmented the metal–metal backbone, and the only isolable products were $[Au(CH_3impy)_2X_2]PF_6$, where X = Br or I. These oxidized products can be intentionally obtained (Scheme 3) by direct oxidation of complex **2** with bromine or iodine to form complexes **8** and **9**, respectively. Treatment of complexes **8** and **9** with various silver benzoates did not produce similar metallic clusters; instead, the complexes underwent instantaneous reductive elimination to reform complex **2**.

The composition of all the aforementioned complexes was unambiguously established on the basis of $^1H$ and $^{13}C$ NMR spectroscopy, elemental analyses, and X-ray crystallography. The spectra of the ligand precursor, $[H(CH_3impy)]PF_6$ (**1**), and the $Au^I$ salt, $[Au(CH_3impy)_2]PF_6$ (**2**), were described earlier.[15b] In the polymeric complexes **3** and **4**, protons of the backbone imidazole ring resonate at $\delta$ = 7.69, 7.22 ppm and at $\delta$ = 7.59, 7.02 ppm, respectively. The *N*-methyl resonances shift upfield to $\delta$ = 3.78 ppm and $\delta$ = 3.59 ppm, respectively, relative to that of **2**, whose corresponding value is $\delta$ = 3.93 ppm. The signals of the pyridyl protons adjacent to the nitrogen atom appear at $\delta$ = 8.64 and 8.65 ppm for **3** and **4**, respectively. The protons on the benzoate ring resonate at $\delta$ = 7.97, 7.48 and 7.40 ppm for **3** and at $\delta$ = 7.92 and 7.08 ppm for **4**. Integration of these signals is consistent with the anticipated 1:1 ratio of benzoate ion/NHC ligand. The $^1H$ NMR spectra of **5** and **7** are very similar, and that of **6** was slightly different due to the number of substituents on the benzoate

  

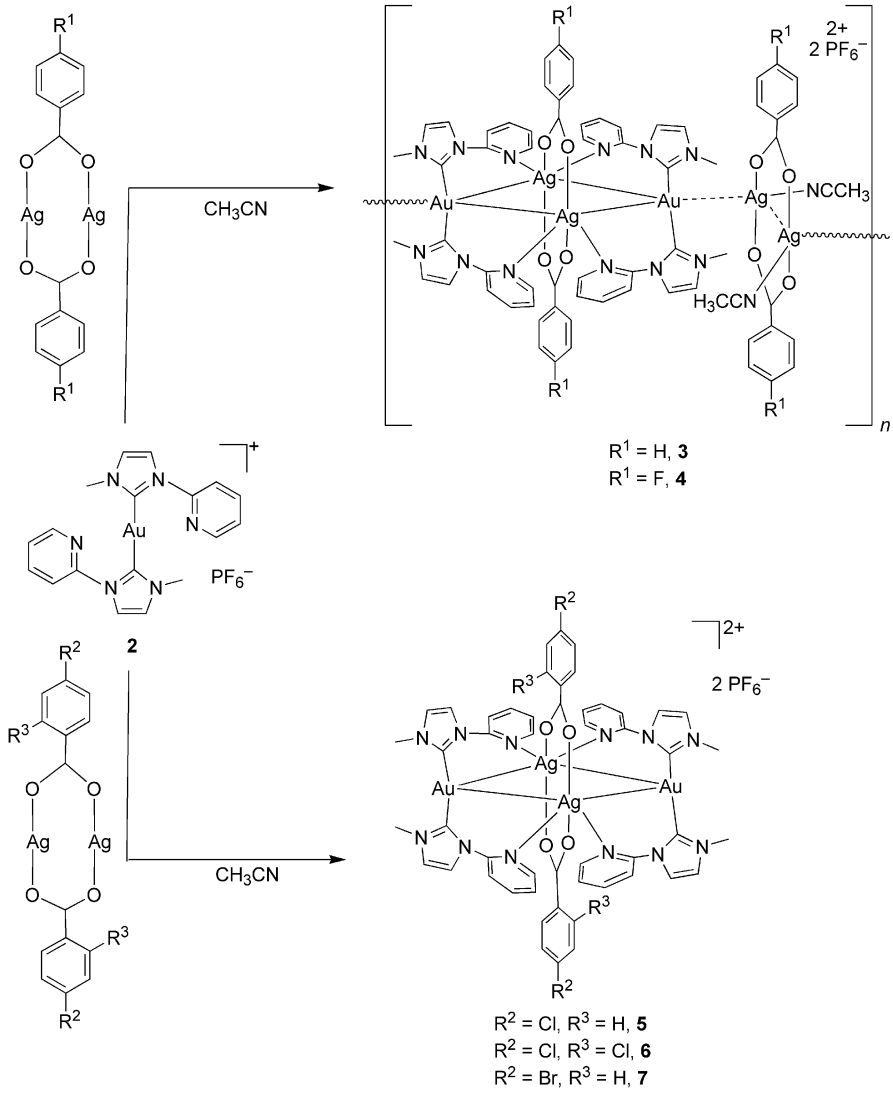


Scheme 2.

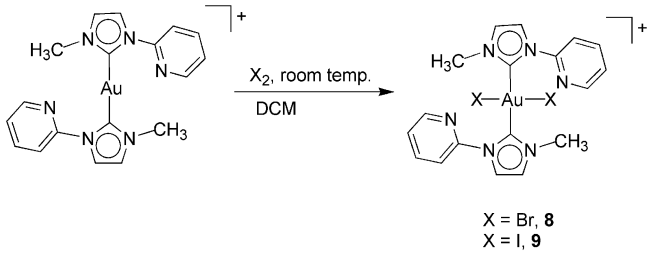


Scheme 3.

ring. For example, the signals of the imidazole backbone protons appear at $\delta$ = 7.66, 7.16 ppm and $\delta$ = 7.75, 7.35 ppm for **5** and **7**, respectively, whereas in **6** the signals of these protons are found at $\delta$ = 7.74 and 7.35 ppm. The *N*-methyl proton resonates at $\delta$ = 3.72, 3.89 and 3.91 ppm for **5**, **6**, and **7**, respectively, also shifted downfield. All of these tetrametallic assemblies exhibit a pair of doublets and a pair of triplets in the aromatic region originating from the pyridyl ring of the NHC ligand. In addition to these, a multiplet at $\delta$ = 7.87 ppm was observed for **5** originating from the benzoate ring. For **6** and **7**, the benzoate-ring protons show discrete resonances for all the unique protons. The $^{13}$C NMR spectra for complexes **3**–**7** reinforce their formulation and are similar to that of **2**, except for the additional peaks in the aromatic region from the carbon atoms of the benzoate ring.

The $Au^{III}$ complexes, **8** and **9**, each display six resonances in the aromatic region of the $^1$H NMR spectrum. Two of them are from the imidazole backbone, and the remaining four are from pyridyl protons. The spectral pattern is very similar to that of **2**, except the resonances of **8** and **9** are slightly shifted downfield. For example, the pyridyl proton adjacent to the nitrogen atom in **8** resonates at $\delta$ = 8.66 ppm and at $\delta$ = 8.60 ppm for **9**, but in **2** it resonates slightly upfield at $\delta$ = 8.50 ppm. The remaining three pyridyl peaks in **8** appear at $\delta$ = 8.09, 7.75 and 7.57 ppm and at $\delta$ = 8.09, 7.75 and 7.55 ppm for **9**. The protons of the imidazole

  

backbone resonate as a doublet at $\delta$ = 7.93 and 7.59 ppm for **8** and at $\delta$ = 7.96 and 7.62 ppm for **9**. The *N*-methyl proton resonances are also shifted downfield and now occur at $\delta$ = 4.17 and 4.07 ppm for **8** and **9**, respectively. The $^{13}C$ NMR spectra for both **8** and **9** are well defined, and each displays the requisite eight resonances in the aromatic region. Five of these are attributed to the pyridyl carbon atom, and the remaining three are associated with the imidazole ring. The *N*-methyl carbon atom resonates at $\delta$ = 39.8 and 40.5 ppm for **8** and **9**, respectively.

X-ray quality crystals of all the complexes **3**–**9**, were successfully obtained by slow vapor diffusion of diethyl ether into acetonitrile solutions of the complexes. The X-ray structure of **2** was published elsewhere.[15b] Both the polymers **3** and **4** have similar structural patterns and crystallize in the triclinic space group $P\bar{1}$. Selected bond lengths and angles for both the polymers are presented in Table 1, whereas plots of the cationic portions are displayed in Figures 1 and 2, respectively. Comparative views of their cores are presented in Figure 6. In **3**, the asymmetric unit consists of one-half of the tetrametallic $Au_2Ag_2$ core associated to one-half of an $Ag_2(CO_2Ph)_2$ unit, a hexafluorophosphate anion and two acetonitrile solvents. The cationic portion contains a tetrametallic core straddling the inversion center. Each $Au^I$ center is nearly linearly coordinated to two NHC ligands with a C(1)–Au(1)–C(10A) angle of 174.14(13)°. Additionally, the $Au^I$ center contacts the pyridyl-bridged $Ag_2$ dimer with Au(1)–Ag(1) and Au(1)–Ag(1A) separations of 3.1958(3) and 3.2154(3) Å and an acute Ag(1)–Au(1)–Ag(1A) angle of 51.035(8)°. The $Au^I$ center is closely connected to the linking $Ag_2$–benzoate dimer with a small Au(1)–Ag(2) separation of only 2.8821(3) Å. The Ag(1)–Ag(1A) separation of 2.7620(5) Å found in the internal $Ag_2$–benzoate dimer is slightly smaller than the Ag(2)–Ag(2A) separation of 2.8509(5) Å found in the connecting $Ag_2$–benzoate dimer. The distance from the centroid of the internal Ag–Ag vector to Au(1) is 2.893 Å. The remaining intermetallic angles vary considerably with 162.018(9)° for Ag(2)–Au(1)–Ag(1), 145.945(8)° for Ag(2)–Au(1)–Ag(1A) and 132.192(18)° for Au(1)–Ag(2)–Ag(2A). The Au(1)–C(1) and Au(1)–C(10) separations are nearly identical at 2.013(3) and 2.012(3) Å, respectively. The Ag–O distances in the internal $Ag_2$ dimer are noticeably longer than those found within the connecting $Ag_2$ dimer with Ag(1)–O(1) and Ag(1)–O(2) measuring 2.230(2) and 2.237(2) Å and Ag(2)–O(3) and Ag(2)–O(4) measuring 2.200(2) and 2.219(3) Å, respectively. The pyridyl groups are twisted relative to their imidazole counterparts by about 28.53° for the C(1)-containing ligand and 38.49° for the C(10)-containing ligand. Interestingly, the pyridyl lone pairs are not directly oriented towards the Ag atoms, and the related C(7)–N(3)–Ag(1) and C(16)–N(6)–Ag(1) angles deviate from their ideal (180°) end-on approach to 159.6 and 150.5°, respectively. This distortion is manifested in large Ag(1)–N(3) and Ag(1)–N(6) separations of 2.564(3) and 2.509(3) Å. Finally, the coordinated acetonitrile is bound more tightly to the linking $Ag_2$–benzoate dimer with an Ag(2)–N(7) separation of 2.452(4) Å.

Table 1. Selected bond lengths [Å] and angles [°] for **3** and **4**.

| Compound **3** | | Compound **4** | |
|---|---|---|---|
| Au(1)–Ag(1) | 3.1958(3) | Au(1)–Ag(1) | 2.9297(4) |
| Au(1)–Ag(1A) | 3.2154(3) | Au(1)–Ag(2A) | 3.2892(4) |
| Au(1)–Ag(2) | 2.8821(3) | Au(1)–Ag(2) | 3.2291(4) |
| Ag(1)–Ag(1A) | 2.7620(5) | Au(2)–Ag(4) | 2.9150(4) |
| Ag(2)–Ag(2A) | 2.8509(5) | Au(2)–Ag(3) | 3.2752(4) |
| Au(1)–C(1) | 2.013(3) | Au(2)–Ag(3A) | 3.2288(4) |
| Ag(1)–N(3) | 2.564(3) | Ag(2)–Ag(2A) | 2.7561(7) |
| Ag(1)–N(6) | 2.509(3) | Ag(1)–Ag(1A) | 2.8366(8) |
| Ag(2)–N(7) | 2.452(4) | Ag(3)–Ag(3A) | 2.7724(7) |
| Ag(1)–O(1) | 2.230(2) | Ag(4)–Ag(4A) | 2.8534(8) |
| Ag(1)–O(2) | 2.237(2) | Au(1)–C(1) | 2.019(5) |
| Ag(2)–O(3) | 2.200(2) | Au(2)–C(42) | 2.004(6) |
| Ag(2)–O(4) | 2.219(3) | Ag(2)–N(6) | 2.529(4) |
| C(19)–O(1) | 1.259(4) | Ag(2)–N(3A) | 2.488(5) |
| C(19)–O(2) | 1.264(4) | Ag(3)–N(9) | 2.590(4) |
| C(26)–O(3) | 1.260(4) | Ag(3)–N(12) | 2.503(4) |
| C(26)–O(4) | 1.251(4) | $Ag_2$centroid–Au(1) | 2.954 |
| $Ag_2$centroid–Au(1) | 2.893 | $Ag_2$centroid–Au(2) | 2.942 |
| | | Ag(1)–Au(1)–Ag(2) | 177.964(13) |
| | | Ag(1)–Au(1)–Ag(2A) | 132.013(12) |
| C(1)–Au(1)–C(10A) | 174.14(13) | Ag(2)–Au(1)–Ag(2A) | 50.016(12) |
| Ag(2)–Au(1)–Ag(1) | 162.018(9) | Ag(4)–Au(2)–Ag(3) | 150.349(13) |
| Ag(2)–Au(1)–Ag(1A) | 145.945(8) | Ag(4)–Au(2)–Ag(3A) | 158.325(13) |
| Ag(1)–Au(1)–Ag(1A) | 51.035(8) | Ag(3)–Au(2)–Ag(3A) | 50.455(12) |
| Ag(1A)–Ag(1)–Au(1) | 64.849(10) | C(1)–Au(1)–C(10) | 176.5(2) |
| Ag(1A)–Ag(1)–Au(1A) | 64.116(10) | C(33)–Au(2)–C(42) | 174.3(2) |
| Au(1)–Ag(1)–Au(1A) | 128.965(8) | Au(1)–Ag(1)–Ag(1A) | 116.68(2) |
| Ag(2A)–Ag(2)–Au(1) | 132.192(18) | Au(2)–Ag(4)–Ag(4A) | 120.98(2) |

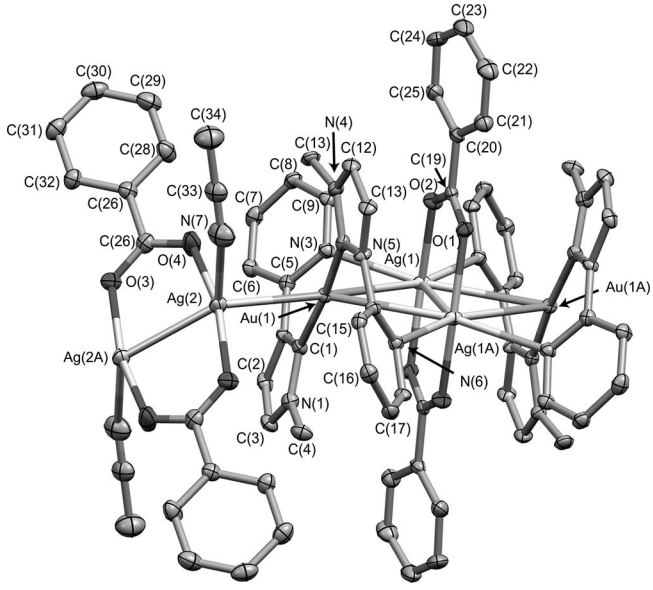


Figure 1. Thermal ellipsoid plot (50%) of the cationic portion of $\{[Au_2Ag_4(CH_3impy)_4(C_6H_5CO_2)_4(CH_3CN)_2](PF_6)_2\}_n$ (**3**), with hydrogen atoms omitted for clarity. The unlabeled atoms are generated by a crystallographically imposed inversion center located between Ag(1) and Ag(1A).

As shown in Figure 2, polymer **4** crystallizes with two cations and two hexafluorophosphate anions, one of them being structurally slightly disordered, in the asymmetric unit. As in **3**, the cations of **4** consist of a tetrametallic $Au_2Ag_2$ core interconnected to an $[Ag(4\text{-fluorobenzoate})]_2$ dimer. Each of these straddles an inversion center making

  

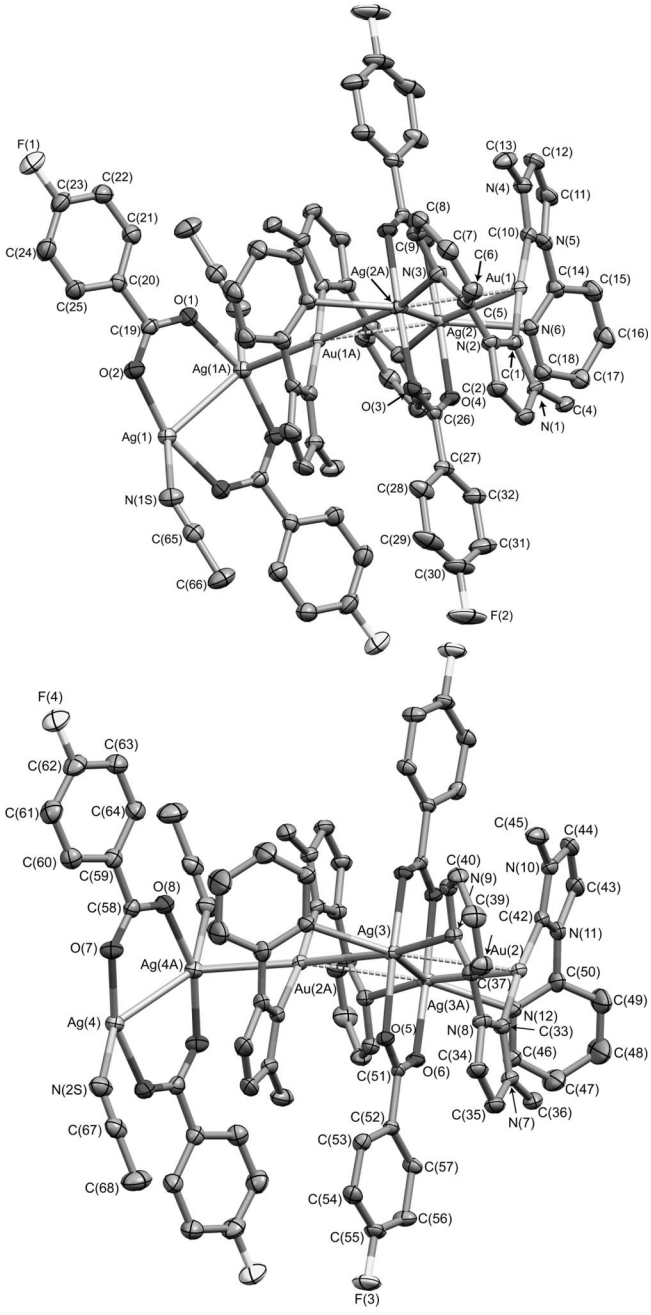


Figure 2. Crystal structure drawings of the two cationic portions of $\{[Au_2Ag_4(CH_3impy)_4(FC_6H_4CO_2)_4(CH_3CN)_2](PF_6)_2\}_n$ (**4**), with ellipsoids drawn at 50% and hydrogen atoms omitted for clarity. The unlabeled atoms are generated by a crystallographically imposed inversion center located between Ag(2) and Ag(2A) (top) and between Ag(3) and Ag(3A) (bottom).

only one-half of each crystallographically unique. The two cations of **4** contain similar metal–metal separations but deviate considerably in their intermetallic angles. For example, in the Au(1)-containing cation, the Au(1)–Ag(2) and Au(1)–Ag(1) separations measuring 3.2291(4) and 2.9297(4) Å, respectively, are close to the related distances in the Au(2)-containing cation where the Au(2)–Ag(3) and Au(2)–Ag(4) distances measure 3.2752(4) and 2.9150(4) Å. Likewise, the Au(1)–Ag(2A) and Au(2)–Ag(3A) separations are similar at 3.2892(4) and 3.2288(4) Å, respectively. The separations between the silver dimers are also close with Ag(2)–Ag(2A) and Ag(3)–Ag(3A) equaling 2.7561(7) and 2.7724(7) Å, and these values are slightly shorter than those found in the connecting [Ag(4-fluorobenzoate)]$_2$ dimer [Ag(1)–Ag(1A) 2.8366(8); Ag(4)–Ag(4A) 2.8534(8) Å]. The distances from the Au atoms to the centroid of the internal [Ag(4-fluorobenzoate)]$_2$ dimer are close at 2.954 Å for Au(1)–Ag(2) Ag(2A)$_{centroid}$ and 2.942 Å for Au(2)–Ag(3)Ag(3A)$_{centroid}$. In contrast, the angles between the diamond core and the connecting [Ag(4-fluorobenzoate)]$_2$ dimer deviate significantly with the Ag(1)–Au(1)–Ag(2) and Ag(1)–Au(1)–Ag(2A) angles measuring 177.964(13) and 132.013(12)°, respectively. The corresponding Ag(4)–Au(2)–Ag(3) and Ag(4)–Au(2)–Ag(3A) angles in the Au(2)-containing cation are more uniform at 150.349(13) and 158.325(13)°, respectively. The internal angles of the diamond cores are also close to each other with Ag(2)–Au(1)–Ag(2A) and Au(1)–Ag(2)–Au(1A) measuring 50.016(12) and 129.984(12)°, which are very close to the corresponding angles in the Au(2)-containing cation with Ag(3)–Au(2)–Ag(3A) and Au(2)–Ag(3)–Au(2A) angles of 50.455(12) and 129.545(12)°. The Ag–O separations in the internal $Ag_2$ dimer (Ag–$O_{ave}$ 2.232 Å) are slightly larger than those in the connecting $Ag_2$ dimer (Ag–$O_{ave}$ 2.193 Å). Like in complex **3** the pyridyl groups are twisted relative to their attached imidazole ring with interplaner angles of 40.67 and 31.87° for the N(2)- and N(4)-containing ligands and 35.28 and 48.52° for the N(7)- and N(11)-containing ligands. Additionally, like in **3**, the pyridyl groups are slightly canted away from the Ag centers, to which they are coordinated with a C(7)–N(3)–Ag(2) angle of 158.15° and a C(16)–N(6)–Ag(2) angle of 150.84°. In the Au(2)-containing cation the C(39)–N(9)–Ag(3) angle measures 153.69°, whereas the C(48)–N(12)–Ag(3) angle at 170.41° is closer to the ideal 180° for direct, linear coordination. Lastly, each $Ag^I$ center of the linking $Ag_2$ dimer is coordinated to an acetonitrile solvate with separations of 2.548(5) Å for Ag(1)–N(1S) and 2.573(5) for Ag(4)–N(2S).

The three tetrametallic assemblies **5**, **6** and **7**, are isostructural and crystallize in the orthorhombic space group *Pccn*. Selected bond lengths and angles are presented in Table 2, whereas thermal ellipsoid plots of the cationic portions are displayed in Figures 3, 4 and 5, respectively. Comparative views of their cores are presented in Figure 6.

In each case, the asymmetric unit contains one half of the cationic portion and one hexafluorophosphate anion. The cations rest on a crystallographic twofold that bisects the central [Ag(benzoate)]$_2$ dimer. In **5**, the central [Ag(4-chlorobenzoate)]$_2$ is flanked by two $Au^I$ centers with fairly long Au(1)–Ag(1) and Au(2)–Ag(1) distances of 3.2888(8) and 3.2307(8) Å. The symmetry-equivalent Ag(1)–Ag(1A) separation is much smaller at 2.7285(14) Å. The centroid of this Ag–Ag vector is 2.992 Å from Au(1) and 2.929 Å from Au(2). The Ag(1)–Au(1)–Ag(1A) intermetallic angle measures 49.02(3)°, whereas the opposing Ag(1)–Au(2)–Ag(1A) angle is very close at 49.96(3)°. The Au(1)–Ag(1)–Au(2) angle is much larger at 130.51(2) Å. This angle is nearly evenly

  

Table 2. Selected bond lengths [Å] and angles [°] for **5**–**7**.

| Compound | **5** | **6** | **7** |
|---|---|---|---|
| Ag(1)–Ag(1A) | 2.7285(14) | 2.7130(7) | 2.7287(5) |
| Ag(1)–Au(2) | 3.2307(8) | 3.2393(5) | 3.2358(3) |
| Ag(1)–Au(1) | 3.2888(8) | 3.3203(5) | 3.3041(3) |
| Au(1)–C(1) | 1.989(10) | 2.013(5) | 2.011(3) |
| Au(2)–C(10) | 2.017(9) | 2.012(5) | 2.013(3) |
| Ag(1)–N(3) | 2.431(8) | 2.435(4) | 2.446(3) |
| Ag(1)–N(6) | 2.447(8) | 2.455(4) | 2.465(3) |
| Ag(1)–O(1) | 2.285(7) | 2.275(3) | 2.285(2) |
| Ag(1)–O(2A) | 2.281(7) | 2.281(3) | 2.262(2) |
| C(19)–O(1) | 1.255(12) | 1.251(6) | 1.255(4) |
| C(19)–O(2) | 1.248(10) | 1.254(6) | 1.260(4) |
| Au···Au | 3.883 | 3.580 | 3.810 |
| $Ag_2$centroid–Au(1) | 2.992 | 3.031 | 3.009 |
| $Ag_2$centroid–Au(2) | 2.929 | 2.942 | 2.934 |
| Ag(1A)–Ag(1)–Au(2) | 65.021(13) | 65.244(7) | 65.062(4) |
| Ag(1A)–Ag(1)–Au(1) | 65.492(13) | 65.887(7) | 65.611(4) |
| Au(2)–Ag(1)–Au(1) | 130.51(2) | 131.130(12) | 130.673(8) |
| Ag(1)–Au(2)–Ag(1A) | 49.96(3) | 49.512(14) | 49.877(9) |
| Ag(1)–Au(1)–Ag(1A) | 49.02(3) | 48.227(13) | 48.778(9) |
| C(1)–Au(1)–Ag(1A) | 104.4(2) | 103.30(13) | 104.96(7) |
| C(1)–Au(1)–C(1A) | 179.6(5) | 179.8(3) | 178.34(14) |
| C(10)–Au(2)–C(10A) | 179.0(5) | 178.2(3) | 178.68(14) |

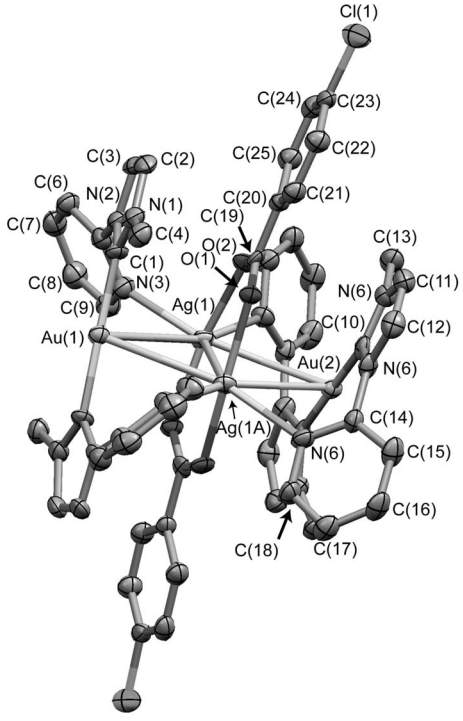


Figure 3. Thermal ellipsoid plot (50%) of the cationic portion of $[Au_2Ag_2(CH_3impy)_4(ClC_6H_4CO_2)_2](PF_6)_2$ (**5**), with hydrogen atoms omitted for clarity. The unlabeled atoms are generated by a crystallographically imposed twofold rotation axis located between Ag(1) and Ag(1A).

bisected by the $[Ag(4\text{-chlorobenzoate})]_2$ dimer with Au(1)–Ag(1)–Ag(1A) and Au(2)–Ag(1)–Ag(1A) angles of 65.492(13) and 65.021(13)°, respectively. Each gold center is nearly linearly coordinated to two NHC moieties with nearly equal C(1)–Au(1)–C(1A) and C(10)–Au(2)–C(10A) angles of 179.6(5) and 179.0(5)°. These moieties are twisted

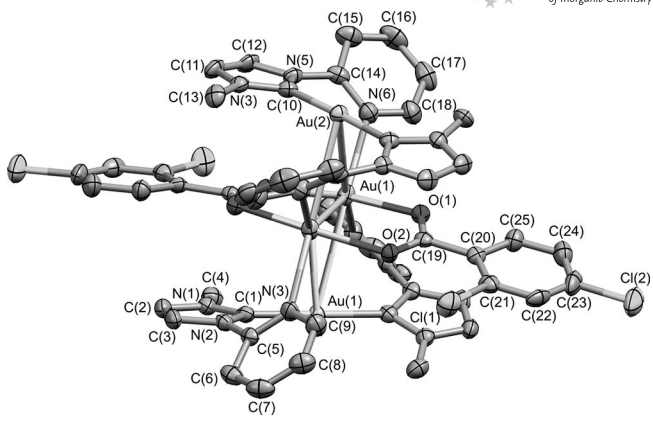


Figure 4. Thermal ellipsoid plot (50%) of the cationic portion of $[Au_2Ag_2(CH_3impy)_4(Cl_2C_6H_3CO_2)_2](PF_6)_2$ (**6**), with hydrogen atoms omitted for clarity. The unlabeled atoms are generated by a crystallographically imposed twofold rotation axis located between Ag(1) and Ag(1A).

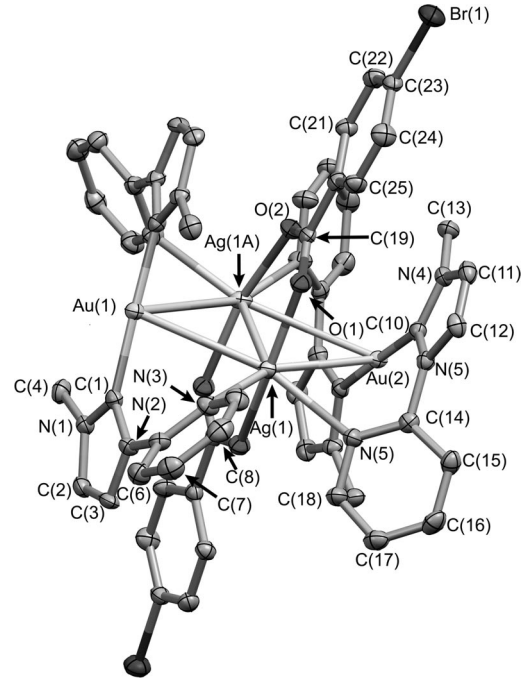


Figure 5. Crystal structure drawing with ellipsoids draw at 50% of the cationic portion of $[Au_2Ag_2(CH_3impy)_4(BrC_6H_4CO_2)_2](PF_6)_2$ (**7**), with hydrogen atoms omitted for clarity. The unlabeled atoms are generated by a crystallographically imposed twofold rotation element bisecting the Ag(1)–Ag(1A) vector.

by 60.44° from each other. Each $Ag^I$ center is coordinated to two oxygen atoms [Ag(1)–O(1) 2.285(7) Å and Ag(1A)–O(2) 2.281(7) Å] and to two pyridyl groups [Ag(1)–N(3) 2.431(8) Å and Ag(1)–N(6) 2.447(8) Å]. The bridging benzoate groups are slightly twisted with respect to each other with an 18.2° angle between the respective $CO_2$ planes. The O(1)–O(2) separation at 2.256 Å is considerably smaller than the Ag–Ag separation causing the O(1)–Ag(1A)–O(2A) and O(2)–Ag(1)–O(1A) angles to contract from the ideal *trans*-spanning angle of 180° to 166.8(2)°. Likewise,

  

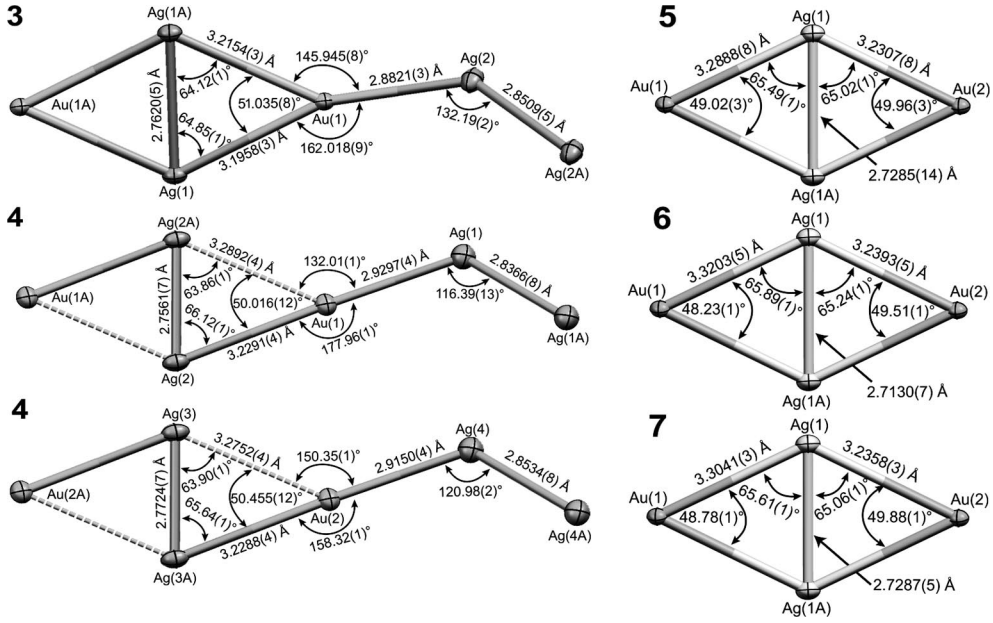


Figure 6. Comparison of the metallic cores of **3**–**7** with selected bond lengths [Å] and angles [°].

the O(1)–C(19)–O(2) angle is slightly expanded from the ideal $sp^2$ geometry to 128.7(9)°; however, the C(19)–O(1) and C(19)–O(2) separations are more regular at 1.255(12) and 1.248(10) Å, respectively. The intermolecular Au···Au interactions are long at 3.883 Å.

The X-ray structure of **6** is very similar to that of **5** except for the additional chloro substitution on the benzoate ring. Like **5**, the cation of **6** resides on a crystallographic twofold axis with Au(1)–Ag(1) and Au(2)–Ag(1) separations of 3.3203(5) and 3.2393(5) Å and a shorter Ag(1)–Ag(1A) distance of 2.7130(7) Å. The centroid of this dimer lies 3.031 Å from Au(1) and 2.942 Å from Au(2). The intermetallic Ag(1)–Au(1)–Ag(1A) and Ag(1)–Au(2)–Ag(1A) angles are acute and measure 48.227(13) and 49.512(14)°, whereas the Au(1)–Ag(1)–Au(2) angle is much larger at 131.130(12)°. The silver dimer almost perfectly bisects this angle with an Au(1)–Ag(1)–Ag(1A) angle of 65.887(7)° and an Au(2)–Ag(1)–Ag(1A) angle of 65.244(7)°. Each $Au^I$ center is nearly linearly coordinated to two NHC ligands with Au(1)–C(1) and Au(2)–C(10) distances of 2.013(5) and 2.012(5) Å and C(1)–Au(1)–C(1A) and C(10)–Au(2)–C(10A) angles of 179.8(3) and 178.2(3)°. These centers are twisted by 59.43° from each other. The central Ag atoms are bridged by the disubstituted benzoate with Ag(1)–O(1) and Ag(1)–O(2A) distances of 2.275(3) and 2.281(3) Å. As observed in **5**, the coordinating $CO_2$ groups of **6** are twisted by 19.4° from each other, whereas the O(1)···O(2) separation at 2.241 Å is smaller than the Ag–Ag separation. The O(1)–C(19) and O(2)–C(19) separations are nearly equal at 1.251(6) and 1.254(6)°, whereas the O(1)–C(19)–O(2) angle measures 126.8(5)°. Each $Ag^I$ center is also coordinated to two pyridyl groups with Ag(1)–N(3) and Ag(1)–N(6) angles of 2.435(4) and 2.455(4) Å and an N(3)–Ag(1)–N(6) angle of 94.59(15)°. The intermolecular Au···Au contacts at 3.580 Å are slightly shorter than those found in **5**.

The metrical parameters for the 4-bromobenzoate-containing complex **7** are very similar to those in **5** and **6** with Au(1)–Ag(1) and Au(2)–Ag(1) separations of 3.3041(3) and 3.2358(3) Å, and an Au(1)–Ag(1)–Au(2) angle of 130.673(8)°. The acute Ag(1)–Au(1)–Ag(1A) angle registers 48.778(9)°, whereas the Ag(1)–Au(2)–Ag(1A) angle is slightly larger at 49.877(9)°. The Au(1)–Ag(1)–Ag(1A) angle at 65.611(4)° is nearly identical to the Au(2)–Ag(1)–Ag(1A) angle that measures 65.062(4)°. The Ag(1)–Ag(1a) separation at 2.7287(5) Å is very close to that of **5**. The centroid of this Ag–Ag vector is 3.009 Å from Au(1) and 2.934 Å from Au(2). Like the previous complexes, each $Au^I$ center is nearly linearly coordinated to two imidazole moieties with C(1)–Au(1)–C(1A) and C(10)–Au(2)–C(10A) angles of 178.34(14) and 178.68(14)°. These centers are twisted by 60.46° from each other. The bridging benzoate binds to the Ag centers with Ag(1)–O(1) and Ag(1A)–O(2) distances of 2.285(2) and 2.262(2) Å and an O(1)–C(19)–O(2) angle of 126.3(3)°. The C(19)–O(1) and C(19)–O(2) distances are 1.255(4) and 1.260(4) Å, respectively, and the O(1)···O(2) distance at 2.244 Å remains shorter than the corresponding Ag–Ag distance. The benzoate groups are slightly twisted with respect to each other as evidenced by the 18.90° angle between the $CO_2$-containing planes. The benzoate O(1)–Ag(1)–O(2A) angle at 166.20(8)° is considerably less than the ideal 180° *trans*-spanning. The pyridyl groups are coordinated to the Ag centers in a *cis* fashion with an N(3)–Ag(1)–N(6) angle of 93.30(9)° and Ag(1)–N(3) and Ag(1)–N(6) separations of 2.446(3) and 2.465(3) Å, respectively. The nearest intermolecular Au···Au interaction at 3.810 Å is very long.

Thermal-ellipsoid plots for the cationic portions of $Au^{III}$ complexes **8** and **9** are shown in Figures 7 and 8, respectively, whereas some selected bond lengths and angles for these complexes are displayed in Table 3. These complexes

  

are isostructural and crystallize in the monoclinic space group *C*2/*c* with one-half of the cation and hexafluorophosphate anion residing on an inversion center in the asymmetric unit. As seen in Figure 7, the cation of **8** contains an $Au^{III}$ metal center oriented in a rigorously square-planar environment with two *trans*-NHC ligands and two *trans*-bromide ions. The Au(1)–C(1) and Au(1)–Br(1) separations are 2.030(4) and 2.4241(4) Å, respectively, and the *cis* C(1)–Au(1)–Br(1) and C(1A)–Au(1)–Br(1) angles at 89.84(10) and 90.16(10)° are very close to the ideal 90°. The imidazole moieties are twisted by 69.35° relative to the $C_2Br_2$ coordination plane and 29.40° relative to the attached pyridyl group. The structure of **9** is nearly superimposable with that of **8**, but **9** has a slightly larger Au(1)–C(1) separation at 2.0379(19) Å and an Au(1)–I(1) distance of 2.61485(13) Å. The *cis* angles reflect the symmetry-imposed square-planer environment with C(1)–Au(1)–I(1) and C(1A)–Au(1)–I(1) measuring 90.09(5) and 89.91(5)°. The angle between the $C_2I_2$ coordination plane at 68.40° is slightly smaller than that of **8**. However, the pyridyl ring is slightly more twisted (36.85°) in **9** compared to the related angle in **8**.

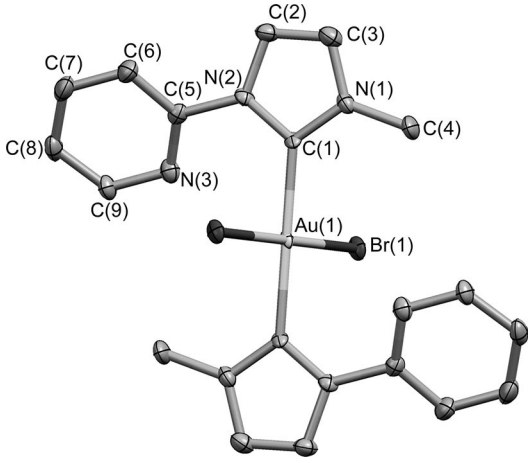


Figure 7. Thermal ellipsoid plot (50%) of the cationic portion of $[Au(CH_3impy)_2Br_2]PF_6$ (**8**), with hydrogen atoms omitted for clarity. Only the crystallographically unique portion is numbered.

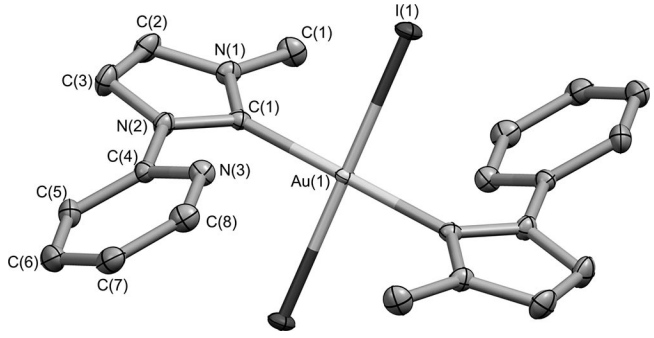


Figure 8. Thermal ellipsoid plot (50%) of the cationic portion of $[Au(CH_3impy)_2I_2]PF_6$ (**9**), with hydrogen atoms omitted for clarity. Only the crystallographically unique portion is numbered.

The electronic absorption spectra for the colorless compounds **3**–**7** are similar and consist of a medium-intensity band between 260 and 270 nm and a more intense shoulder deep into the UV region between 219 and 240 nm. Complexes **8** and **9** are colored, and the spectral pattern is different from what is observed for **3**–**7**. For example, the yellow **8** shows a low-intensity shoulder at 302 nm in addition to two more intense peaks at 266 and 220 nm. In the orange complex **9** only two peaks are observed at 372 and 243 nm. All the UV absorption bands and their respective extinction coefficients for all the compounds are listed in the Experimental Section.

Table 3. Selected bond lengths [Å] and angles [°] for **8** and **9**.

| Compound **8** | | Compound **9** | |
|---|---|---|---|
| Au(1)–C(1) | 2.030(4) | Au(1)–C(1) | 2.0379(19) |
| Au(1)–Br(1) | 2.4241(4) | Au(1)–I(1) | 2.61485(13) |
| C(1)–N(1) | 1.340(5) | C(1)–N(1) | 1.340(2) |
| C(1)–N(2) | 1.354(5) | C(1)–N(2) | 1.355(3) |
| C(1)–Au(1)–C(1A) | 180.00(11) | C(1)–Au(1)–C(1A) | 180.00(5) |
| C(1)–Au(1)–Br(1) | 89.84(10) | C(1)–Au(1)–I(1) | 90.09(5) |
| C(1A)–Au(1)–Br(1) | 90.16(10) | C(1A)–Au(1)–I(1) | 89.91(5) |

Both solution and solid-state samples for the compounds **3**–**7** do not exhibit any noticeable photoluminescence at room temperature, but surprisingly in frozen acetonitrile solution of the compounds (77 K), all of them display intense photoluminescence (Figure 9). The intensity of the photoluminescence is independent of the concentration of the compounds in their frozen solutions. In the polymeric species **3** and **4**, the emission maxima were recorded at 487 ($\lambda_{ex}$ = 368 nm) and 491 nm ($\lambda_{ex}$ = 365 nm), respectively. In case of the tetrametallic assemblies, the emission band undergoes a small redshift in comparison to the polymers. For example, the emission band for **5**, **6** and **7** occurs at 506 ($\lambda_{ex}$ = 397 nm), 500 ($\lambda_{ex}$ = 378 nm) and 505 nm ($\lambda_{ex}$ = 380 nm),

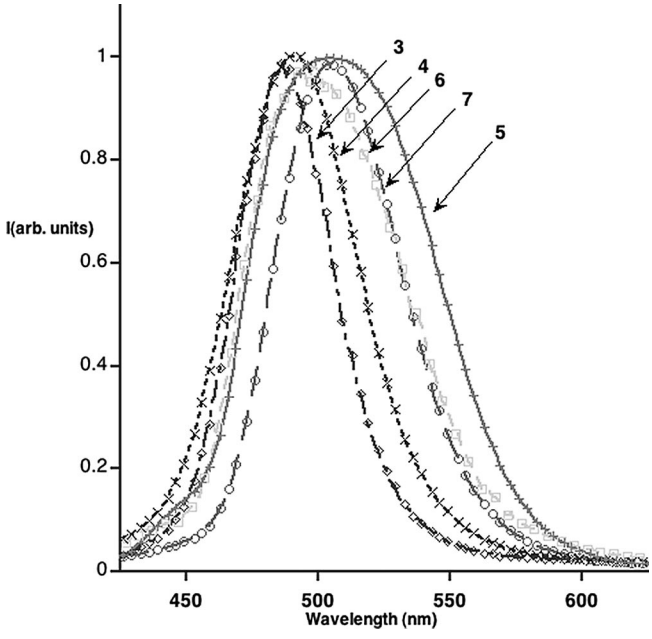


Figure 9. Normalized emission plots for complexes **3**–**7** in frozen acetonitrile (77 K).

  

respectively. No noticeable photoluminescence was observed with acetonitrile solutions of the $Au^{III}$ complexes **8** and **9**, neither at room temperature nor at 77 K.

## Discussion

Unlike our previous work, where the addition of simple $Ag^{I}$ salts to $[Au(CH_3impy)_2]^+$ leads exclusively to linear-chain polymers, the incorporation of benzoate anions produces two distinct structural motifs. The silver salts of benzoic acid or 4-fluorobenzoic acid produce polymeric systems (**3** and **4**) where tetrametallic $Ag_2Au_2$ cores are interconnected by $Ag_2$(benzoate)$_2$ dimers. However, the silver 4-chloro-, 2,4-dichloro- and 4-bromobenzoate salts reproducibly produce discrete $Ag_2Au_2$ tetrametallic complexes. The reason for this discrimination is not fully understood, but it does not appear to be related to simple steric arguments because these groups are oriented away from any congestion. The Hammett $\sigma_p$ parameters[17] are ordered H < F < Cl < Br, which is consistent with grouping complexes **3** and **4** together and **5** and **7** together. Further, the corresponding Ag–Ag separations in the central $Ag_2$(benzoate)$_2$ dimers follow this trend with **3** ≈ **4** > **5** ≈ **7** > **6**. The smallest separation [2.7130(7) Å] is found in the $Cl_2$-benzoate-containing species **6**, whereas larger separations [2.7724(7)–2.7561(7) Å] are observed in **3** and **4**. Intermediate are the Ag–Ag separations of **5** and **7**, which are nearly identical at 2.7285(14) and 2.7287(5) Å. Likewise, the Ag–pyridyl separations decrease as the Ag–Ag separation decreases following the Hammett series suggesting greater participation of the pyridyl group in synergistic bonding. In **3** and **4** the Ag–Ag separations in the linking $Ag_2$(benzoate)$_2$ dimers at ca. 2.85 Å are much larger; however, here each $Ag^{I}$ atom is only three-coordinate, not counting the Ag–Ag interaction. Interestingly, the chemistry with electron-donating substituted silver benzoates (methyl and methoxy) is different, and we have yet to cleanly isolate these products.

The tetrametallic structural motif is not unique, and numerous $Au_2Ag_2R_2L_2$ compounds are found in the literature.[18] For example, Usón and co-workers[19] reported the orange compound $\{Au_2(C_6F_5)_2Ag_2(SC_4H_8)_2\}_n$, which contains very small Ag–Au separations of 2.889 and 2.717 Å. The lack of a bridging ligand keeps the Ag–Ag separation large at 3.05 Å. These units are interconnected by short aurophilic linkages of 2.889 Å generating a polymeric structure. This work was expanded greatly to include a large variety of auxiliary ligands on Ag; however, the overall structure remains the same again with small Au–Ag separations ranging from 2.702 to 2.792 Å and aurophilic connections of 2.889 and 3.013 Å.[20] Fernández et al.[21] furthered this chemistry to include bridging trifluoroacetate groups across the $Ag_2$ dimer, and, although the overall metallic substructure is slightly different, comparison about the silver centers are still valid. In these systems the separation between the Ag atoms of the internal $Ag_2$ dimer is still large compared to complexes **3**–**7**. In $\{Au(C_6F_5)_2Ag(CF_3CO_2)(tht)\}_n$ the Ag–Ag separation is 2.8792(5) Å, whereas in $\{Au(3,5\text{-}C_6Cl_2F_3)_2Ag_2(CF_3CO_2)(tht)\}_n$ the corresponding measurement is slightly smaller at 2.8623(6) Å, and finally in the perchlorophenyl derivative $\{Au(C_6Cl_5)_2Ag(CF_3CO_2)(tht)\}_n$ a larger Ag–Ag separation [2.96615(19) Å] is found. The Au–Ag separations, however, are generally smaller and range from 2.8784(5) to 3.0221(6) Å. A similar trend was observed in the mesitylgold(I) system.[22]

Complexes **3**–**7** are photoluminescent in frozen acetonitrile at 77 K but are non-emissive at room temperature. There is little change in the emission spectra of these complexes; however, a trend similar to the one observed describing their structural difference is noticed. Complexes **3** and **4** have the most blueshifted emission maxima at ca. 490 nm, whereas **5** and **7** have nearly identical spectra that are the most redshifted to ca. 506 nm. The dichlorobenzoate-containing **6** is intermediate. Likewise, the excitations are similarly distributed, with complexes **3** and **4** having nearly identical excitation spectra that consist of a single peak at 365 and 368 nm, respectively, whereas complexes **5**–**7** have a slightly broader profile with major peaks at 380 nm and shoulders towards the blue portion of the electromagnetic spectrum.

Fernández et al.[3] very thoroughly examined the origin of the photophysical properties of $Au_2(C_6F_5)_4Ag_2(OCMe_2)_2$. At high concentrations and in the solid state the emission of this species originates from the aurophilic Au···Au intermolecular interactions; however, in dilute solution, the emission appears to arise from either ππ* or π-MMLCT excited state. Given the similarity in emission profiles in compounds **3**–**7** and the lack of Au···Au interactions in **3** and **4**, a metal-centered (dσ*–pσ) transition is unlikely. In later work, Fernández et al.[23] explored the acetonitrile complexes $Au_2(C_6F_5)_4Ag_2(NCCH_3)_2$ and $Au_2(C_6F_5)_4Cu_2(NCCH_3)_2$ and proposed a similar dσ*–pσ transition to explain their observations at high concentrations or in the solid state. Interestingly, the authors also found a "transition located within the tetranuclear core whose energy is influenced by molecular aggregation." A similar process could be at play in this work; however, here, the energy of the LUMO would be tuned by the benzoate ligand and not aggregation. Such an assignment requires a more thorough investigation and is beyond the scope of this work.

Finally, attempts to oxidize the clusters lead only to disruption of the polymetallic cores and isolation of the monometallic $Au^{III}$ species. It is interesting to note that in **8** and **9** the pyridyl groups of the NHC ligand remain uncoordinated. This is in marked contrast to the related work by Chen and Lin[24] on the related dipyridyl-substituted NHC $impy_2$ where the $d^8$ $Pd^{II}$ center forms a rigid chelate ring that is difficult to open. Faller, Crabtree, and co-workers[25] further elaborated on the chelating ability of pyridyl-substituted NHC ligands and thoroughly explored their ability to interconvert from a C2-bound NHC to a C4-bound NHC on a high-oxidation-state metal atom. The uncoordinated pyridyl groups in **8** and **9** open the possibility of forming $d^8$ coordination polymers by coordinating to another metal atom in a fashion analogous to that shown in Scheme 1. We are currently exploring these reactions.

  

## Conclusions

The chemistry presented here further illustrates the diversity in coordination chemistry of the $CH_3$impy ligand and the sensitivity of auxiliary coordination on the overall structural motif. Incorporation of a benzoate anion does not produce linear coordination polymers, but instead produces two distinct structural motifs. Alteration of the electron-withdrawing groups on the benzoate backbone influences both metrical parameters of the multimetallic complexes as well as the luminescence.

## Experimental Section

**General:** Solvents were used as received without purification or drying. Silver benzoate was obtained from Alfa Aesar. Other silver salts used in this work were synthesized according to a reported[26] procedure, starting from the respective benzoic acids, which were obtained from Acros Organics. 1-Methylimidazole and 2-bromopyridine were obtained from Aldrich. The preparation of Au(tht)Cl is described elsewhere,[27] and the preparations of the imidazolium salt $[HCH_3imPy]PF_6$ and the Au complex $[Au(CH_3impy)_2]PF_6$ were modified from published procedures.[15b] $^1H$ NMR spectra were recorded with a Varian Unity+ NMR spectrometer operating at 500 MHz at 25 °C. Chemical shifts are reported relative to TMS but were measured on the basis of the internal solvent peak. UV/Vis spectra were obtained with an Agilent 8453 UV/Vis spectrophotometer (1 cm cell pathlength). Emission data were recorded with a Spex Fluoromax steady-state fluorimeter. Elemental analyses were performed by Columbia Analytical Services (formally Desert Analytics) in Tucson, AZ.

**Preparation of $[H(CH_3impy)]PF_6$ (1):** 1-Methylimidazole (1.64 g, 20.0 mmol) and 2-bromopyridine (3.16 g, 20.0 mmol) were introduced into a pressure tube. The pressure tube was then capped and placed in an oil bath, whose temperature was maintained at 165 °C. The mixture was stirred for 48 h. After cooling, the resulting oil was transferred to a beaker containing water (15 mL). The mixture was treated with a saturated aqueous solution of $NH_4PF_6$ (50.0 mmol), and a brown yellow solid precipitated. The solid was filtered and washed first with three 15 mL portions of water to remove excess $NH_4PF_6$ and $NH_4Br$ and then with another three 10 mL portions of THF to remove the brown yellow impurity. Product **1** was obtained as an off-white powder in 53% yield (3.24 g). $^1H$ NMR (499.8 MHz, $CD_3CN$, 25 °C): $\delta$ = 9.24 (s, 1 H), 8.59 (m, 1 H), 8.12 (m, 1 H), 8.06 (m, 1 H), 7.72 (d, $J$ = 9.0 Hz, 1 H), 7.57 (m, 1 H), 7.55 (m, 1 H), 3.97 (s, 3 H) ppm. $^{13}C$ NMR (125.7 MHz, $CD_3CN$, 25 °C): $\delta$ = 150.6, 147.5, 141.6, 135.6, 126.4, 125.8, 120.3, 115.1, 37.5 ppm.

**Preparation of $[Au(CH_3impy)_2]PF_6$ (2):** A 100 mL round-bottomed flask was charged with Au(tht)Cl (0.255 g, 0.795 mmol), $[HCH_3impy]PF_6$ (0.485 g, 1.59 mmol), $CH_3COONa$ (0.131 g, 1.59 mmol) and $CH_3CN$ (about 50 mL). The mixture was refluxed for 48 h. After cooling, the solution was filtered through Celite, and the clear filtrate was concentrated to a minimum volume under vacuum. The pale yellow product **2** was precipitated with $Et_2O$ to afford 0.462 g (0.699 mmol) in 88% yield. $^1H$ NMR (499.8 MHz, $CD_3CN$, 25 °C): $\delta$ = 8.50 (d, $J$ = 4.0 Hz, 2 H), 8.00 (d, $J$ = 8.0 Hz, 2 H), 7.87 (t, $J$ = 7.5 Hz, 2 H), 7.76 (d, $J$ = 1.7 Hz, 2 H), 7.47 (t, $J$ = 5.0 Hz, 2 H), 7.37 (d, $J$ = 1.7 Hz, 2 H), 3.93 (s, 6 H) ppm. $^{13}C$ NMR (125.7 MHz, $CD_3CN$, 25 °C): $\delta$ = 183.5, 151.7, 150.1, 140.3, 125.4, 124.8, 121.9, 118.7, 39.5 ppm.

**Preparation of $\{[Au_2Ag_4(CH_3impy)_4(C_6H_5CO_2)_4(CH_3CN)_2](PF_6)_2\}_n$ (3):** A 50 mL round-bottomed flask was charged with $[Au(CH_3impy)_2]PF_6$ (0.052 g, 0.079 mmol), silver benzoate (0.040 g, 0.174 mmol) and $CH_3CN$ (about 30 mL). A reflux condenser was attached to the flask, and the solution was refluxed overnight. The solution was then cooled to room temperature and filtered through Celite. The pale yellow filtrate was concentrated to a minimum volume, and the product was precipitated with $Et_2O$ to afford 0.062 g (0.027 mmol) of **3** as an off-white powder in 68% yield. $C_{68}H_{62}Ag_4Au_2F_{12}N_{14}O_8P_2$ (2318.67): calcd. C 35.22, H 2.69, N 8.45; found C 34.72, H 2.67, N 8.81. $^1H$ NMR (499.8 MHz, $CD_3CN$, 25 °C): $\delta$ = 8.64 (d, $J$ = 6.0 Hz, 4 H), 7.97 (d, $J$ = 7.5 Hz, 8 H), 7.95 (m, 4 H), 7.91 (d, $J$ = 8.0 Hz, 4 H), 7.69 (d, $J$ = 2.0 Hz, 4 H), 7.55 (m, 4 H), 7.48 (t, $J$ = 7.0 Hz, 4 H), 7.40 (t, $J$ = 7.5 Hz, 8 H), 7.22 (d, $J$ = 2.0 Hz, 4 H), 3.78 (s, 12 H) ppm. $^{13}C$ NMR (125.7 MHz, $CD_3CN$, 25 °C): $\delta$ = 183.5, 151.5, 150.6, 141.0, 131.6, 131.1, 128.8, 125.8, 125.0, 122.1, 119.4, 118.1, 39.4 ppm. UV/Vis ($CH_3CN$): $\lambda_{max}$ ($\varepsilon$) = 219 (sh, 71000), 267 (31000) nm.

**Preparation of $\{[Au_2Ag_4(CH_3impy)_4(FC_6H_4CO_2)_4(CH_3CN)_2](PF_6)_2\}_n$ (4):** $[Au(CH_3impy)_2]PF_6$ (0.056 g, 0.085 mmol) and silver 4-fluorobenzoate (0.046 g, 0.188 mmol) were placed in a 50 mL round-bottomed flask, and $CH_3CN$ (30 mL) was added. The solution was stirred at room temperature overnight. After that, the solution was filtered through Celite. The clear filtrate was concentrated to a minimum volume, and $Et_2O$ was added to obtain 0.075 g (0.032 mmol) of **4** as a pale yellow powder in 76% yield. $C_{68}H_{58}Ag_4Au_2F_{16}N_{14}O_8P_2$ (2390.64): calcd. C 34.16, H 2.44, N 8.20; found C 34.13, H 2.40, N 8.20. $^1H$ NMR (499.8 MHz, $CD_3CN$, 25 °C): $\delta$ = 8.65 (d, $J$ = 2.0 Hz, 4 H), 7.98 (t, $J$ = 8.0 Hz, 4 H), 7.92 (m, 8 H), 7.79 (d, $J$ = 8.0 Hz, 4 H), 7.59 (d, $J$ = 2.0 Hz, 4 H), 7.55 (t, $J$ = 6.5 Hz, 4 H), 7.08 (m, 8 H), 7.02 (d, $J$ = 2.0 Hz, 4 H), 3.59 (s, 12 H) ppm. $^{13}C$ NMR (125.7 MHz, $CD_3CN$, 25 °C): $\delta$ = 183.4, 150.9, 141.5, 133.5, 133.4, 125.9, 125.1, 122.1, 119.9, 115.5, 115.3, 39.2 ppm. UV/Vis ($CH_3CN$): $\lambda_{max}$ ($\varepsilon$) = 220 (sh, 68000), 266 (32000) nm.

**Preparation of $[Au_2Ag_2(CH_3impy)_4(ClC_6H_4CO_2)_2](PF_6)_2$ (5):** $[Au(CH_3impy)_2]PF_6$ (0.056 g, 0.084 mmol), silver 4-chlorobenzoate (0.049 g, 0.185 mmol) and $CH_3CN$ (30 mL) were placed in a 50 mL round-bottomed flask. A reflux condenser was attached to the flask, and the solution was refluxed overnight. The solution was then cooled to room temperature and filtered through Celite. The clear filtrate was concentrated, and 0.055 g (0.030 mmol) of product **5** was obtained by precipitating with $Et_2O$ in 71% yield. $C_{50}H_{44}Ag_2Au_2Cl_2F_{12}N_{12}O_4P_2$ (1847.49): calcd. C 32.50, H 2.40, N 9.09; found C 32.80, H 2.37, N 9.28. $^1H$ NMR (499.8 MHz, $CD_3CN$, 25 °C): $\delta$ = 8.60 (d, $J$ = 6.0 Hz, 4 H), 7.95 (t, $J$ = 8.0 Hz, 4 H), 7.87 (m, 8 H), 7.66 (d, $J$ = 2.0 Hz, 4 H), 7.53 (t, $J$ = 5.0 Hz, 4 H), 7.37 (d, $J$ = 8.0 Hz, 4 H), 7.16 (d, $J$ = 2.0 Hz, 4 H), 3.72 (s, 12 H) ppm. $^{13}C$ NMR (125.7 MHz, $CD_3CN$, 25 °C): $\delta$ = 183.5, 151.5, 150.5, 140.9, 132.7, 128.8, 125.7, 125.0, 122.1, 119.3, 119.0, 39.4 ppm. UV/Vis ($CH_3CN$): $\lambda_{max}$ ($\varepsilon$) = 230 (sh, 61000), 267 (38000) nm.

**Preparation of $[Au_2Ag_2(CH_3impy)_4(Cl_2C_6H_3CO_2)_2](PF_6)_2$ (6):** A 50 mL round-bottomed flask was charged with $[Au(CH_3impy)_2]PF_6$ (0.054 g, 0.082 mmol), silver 2,4-dichlorobenzoate (0.054 g, 0.181 mmol) and $CH_3CN$ (30 mL). The solution was stirred at room temperature overnight and then filtered through Celite. The clear filtrate was concentrated to one-third of its initial volume, and then $Et_2O$ was added to precipitate 0.064 g (0.033 mmol) of **6** as a powder in 81% yield. $C_{50}H_{42}Ag_2Au_2Cl_4F_{12}N_{12}O_4P_2$ (1916.38):

  

calcd. C 31.33, H 2.20, N 8.77; found C 31.35, H 2.16, N 9.04. $^1$H NMR (499.8 MHz, $CD_3CN$, 25 °C): $\delta$ = 8.54 (m, 4 H), 7.97 (d, $J$ = 8.0 Hz, 4 H), 7.90 (t, $J$ = 7.6 Hz, 4 H), 7.74 (d, $J$ = 2.0 Hz, 4 H), 7.56 (d, $J$ = 8.0 Hz, 2 H), 7.50 (m, 4 H), 7.43 (d, $J$ = 2.4 Hz, 2 H), 7.35 (d, $J$ = 2.0 Hz, 4 H), 7.27 (d, $J$ = 6.4 Hz, 2 H), 3.89 (s, 12 H) ppm. $^{13}$C NMR (125.7 MHz, $CD_3CN$, 25 °C): $\delta$ = 183.4, 151.6, 150.4, 140.7, 132.4, 130.4, 127.6, 125.6, 125.0, 122.1, 119.1, 39.5 ppm. UV/Vis ($CH_3CN$): $\lambda_{max}$ ($\varepsilon$) = 240 (sh, 34000), 265 (31000) nm.

**Preparation of $[Au_2Ag_2(CH_3impy)_4(BrC_6H_4CO_2)_2](PF_6)_2$ (7):** A 50 mL round-bottomed flask was charged with $[Au(CH_3impy)_2]PF_6$ (0.052 g, 0.079 mmol), silver 4-bromobenzoate (0.053 g, 0.174 mmol) and $CH_3CN$ (30 mL). A reflux condenser was attached to the flask, and the solution was refluxed overnight. The solution was then cooled to room temperature and filtered through Celite. The pale yellow filtrate was concentrated to a minimum volume, and the product was precipitated with $Et_2O$ to afford 0.056 g (0.029 mmol) of **7** as an off-white powder in 73% yield. $C_{50}H_{44}Ag_2Au_2Br_2F_{12}N_{12}O_4P_2$ (1936.39): calcd. C 31.01, H 2.29, N 8.68; found C 30.67, H 2.40, N 9.30. $^1$H NMR (499.8 MHz, $CD_3CN$, 25 °C): $\delta$ = 8.53 (d, $J$ = 7.6 Hz, 4 H), 7.99 (d, $J$ = 8.0 Hz, 4 H), 7.89 (m, 8 H), 7.75 (d, $J$ = 2.0 Hz, 4 H), 7.49 (m, 8 H), 7.35 (d, $J$ = 2.0 Hz, 4 H), 3.91 (s, 12 H) ppm. $^{13}$C NMR (125.7 MHz, $CD_3CN$, 25 °C): $\delta$ = 183.5, 151.6, 150.4, 140.7, 132.9, 131.8, 125.6, 124.9, 122.0, 119.1, 39.4 ppm. UV/Vis ($CH_3CN$): $\lambda_{max}$ ($\varepsilon$) = 237 (sh, 48000), 267 (35000) nm.

**Preparation of $[Au(CH_3impy)_2Br_2]PF_6$ (8):** A 100 mL round-bottomed flask was charged with $[Au(CH_3impy)_2]PF_6$ (0.102 g, 0.155 mmol) and dichloromethane (40 mL). Bromine (0.037 g, 0.232 mmol) was placed in another flask, containing dichloromethane (10 mL), and the mixture was stirred to form a homogeneous solution. To the rapidly stirred solution of $[Au(CH_3impy)_2]PF_6$, the dichloromethane solution of bromine was added dropwise. After completion of the addition, the solution was stirred at room temperature overnight. The insoluble compound **8** separated, was filtered and washed with two 10 mL portions of dichloromethane to remove any excess bromine. The compound was dried under vacuum to obtain 0.115 g (0.141 mmol) of **8** as a yellow powder in 91% yield. $C_{18}H_{18}AuBr_2F_6N_6P$ (820.13): calcd. C 26.36, H 2.21, N 10.24; found C 26.05, H 2.18, N 9.94. $^1$H NMR (499.8 MHz, $CD_3CN$, 25 °C): $\delta$ = 8.66 (d, $J$ = 7.0 Hz, 2 H), 8.09 (t, $J$ = 7.5 Hz, 2 H), 7.93 (d, $J$ = 2.5 Hz, 2 H), 7.75 (d, $J$ = 8.0 Hz, 2 H), 7.59 (d, $J$ = 2.5 Hz, 2 H), 7.57 (t, $J$ = 5.5 Hz, 2 H), 4.17 (s, 6 H) ppm. $^{13}$C NMR (125.7 MHz, $CD_3CN$, 25 °C): $\delta$ = 150.9, 150.4, 149.8, 141.4, 127.2, 125.9, 123.2, 117.5, 39.8 ppm. UV/Vis ($CH_3CN$): $\lambda_{max}$ ($\varepsilon$) = 220 (61000), 266 (14000), 302 (sh, 4000) nm.

**Preparation of $[Au(CH_3impy)_2I_2]PF_6$ (9):** A 100 mL round-bottomed flask was charged with $[Au(CH_3impy)_2]PF_6$ (0.102 g, 0.155 mmol) and dichloromethane (40 mL). Iodine (0.059 g, 0.233 mmol) was placed in another flask, containing dichloromethane (10 mL), and the mixture was stirred to form a homogeneous solution. The dichloromethane solution of iodine was then added dropwise to the rapidly stirred solution of $[Au(CH_3impy)_2]PF_6$. The solution was stirred at room temperature overnight. Compound **9** was insoluble in dichloromethane and precipitated from the solution. The solid was filtered and washed with two 10 mL portions of dichloromethane to remove excess iodine. The product was dried under vacuum to obtain 0.133 g (0.146 mmol) of **9** as an orange powder in 94% yield. $C_{18}H_{18}AuF_6I_2N_6P$ (914.13): calcd. C 23.65, H 1.98, N 9.19; found C 23.80, H 1.96, N 9.15. $^1$H NMR (499.8 MHz, $CD_3CN$, 25 °C): $\delta$ = 8.60 (d, $J$ = 2.5 Hz, 2 H), 8.09 (t, $J$ = 9.0 Hz, 2 H), 7.96 (d, $J$ = 2.5 Hz, 2 H), 7.75 (d, $J$ = 8.5 Hz, 2 H), 7.62 (d, $J$ = 2.5 Hz, 2 H), 7.55 (t, $J$ = 5.0 Hz, 2 H), 4.07 (s, 6 H) ppm. $^{13}$C NMR (125.7 MHz, $CD_3CN$, 25 °C): $\delta$ = 150.6, 149.6, 145.1, 141.3, 127.4, 125.8, 123.5, 117.6, 40.5 ppm. UV/Vis ($CH_3CN$): $\lambda_{max}$ ($\varepsilon$) = 243 (33000), 372 (5000) nm.

**X-ray Crystallography:** X-ray quality crystals were obtained by slow vapor diffusion of diethyl ether into an acetonitrile solution of the respective complex. In each case, suitable crystals were chosen, coated with a hydrocarbon oil and mounted on a glass fiber. X-ray crystallographic data were collected at low temperature (100 K) with a Bruker SMART Apex CCD diffractometer using Mo-$K_\alpha$ radiation and a detector-to-crystal distance of 4.94 cm. Data collections were optimized for maximum coverage and redundancy with 0.5° scans in $\omega$ and $\phi$ and an exposure time ranging from 10 to 25 s per frame. The $2\theta$ ranges extended from 3.0 to 64°. Data were corrected for Lorentz and polarization effects by using the SAINT program and corrected for absorption by using SADABS. Unit cells were indexed by using up to 9999 reflections harvested from the data collection. The structures were solved by direct methods and refined by using the SHELXTL 6.10 software package.[28] Crystallographic data for complexes **3**–**7** and **8**–**9** are presented in Tables 4 and 5, respectively. CCDC-713346 (for **3**), -713347 (for **4**), -713348 (for **5**), -713349 (for **6**), -713350 (for **7**), -713351 (for **8**), -713352 (for **9**) contain the supplementary crystallographic data for this paper. These data can be obtained free of charge from The Cambridge Crystallographic Data Centre via www.ccdc.cam.ac.uk/data_request/cif.

Table 4. X-ray crystallographic data for complexes **3**–**7**.

| Compound | **3**·2$CH_3CN$ | **4**·2$CH_3CN$ | **5** | **6** | **7** |
|---|---|---|---|---|---|
| Empirical formula | $C_{36}H_{34}Ag_2AuF_6N_8O_4P$ | $C_{68}H_{58}Ag_4Au_2F_{16}N_{14}O_8P_2$ | $C_{50}H_{44}Ag_2Au_2Cl_2F_{12}N_{12}O_4P_2$ | $C_{50}H_{42}Ag_2Au_2Cl_4F_{12}N_{12}O_4P_2$ | $C_{50}H_{44}Ag_2Au_2Br_2F_{12}N_{12}O_4P_2$ |
| Formula mass | 1200.39 | 2390.64 | 923.74 | 1916.37 | 1936.40 |
| Crystal system | triclinic | triclinic | orthorhombic | orthorhombic | orthorhombic |
| Space group | $P\bar{1}$ | $P\bar{1}$ | *Pccn* | *Pccn* | *Pccn* |
| $a$ [Å] | 10.9374(2) | 13.3773(2) | 22.6291(7) | 23.1458(3) | 22.5633(5) |
| $b$ [Å] | 13.6043(2) | 14.2645(2) | 12.9898(5) | 13.3946(2) | 13.1741(3) |
| $c$ [Å] | 14.2812(2) | 21.8991(4) | 19.6085(7) | 19.1046(2) | 19.5070(4) |
| $\alpha$ [°] | 82.2010(10) | 102.8580(10) | 90 | 90 | 90 |
| $\beta$ [°] | 79.6540(10) | 106.4810(10) | 90 | 90 | 90 |
| $\gamma$ [°] | 69.6320(10) | 101.5970(10) | 90 | 90 | 90 |
| $V$ [Å$^3$] | 1953.55(5) | 3747.42(10) | 5763.9(4) | 5922.98(13) | 5798.5(2) |
| $Z$ | 2 | 2 | 4 | 4 | 4 |
| Temperature [K] | 100(2) | 100(2) | 100(2) | 100(2) | 100(2) |
| $R_1$ | 0.0334 | 0.0379 | 0.0494 | 0.0326 | 0.0242 |
| $wR_2$ [$I>2\sigma(I)$] | 0.0545 | 0.0928 | 0.1142 | 0.0752 | 0.0569 |

  

Table 5. X-ray crystallographic data for complexes **8** and **9**.

| Compound | **8** | **9** |
|---|---|---|
| Empirical formula | $C_{18}H_{18}AuBr_2F_6N_6P$ | $C_{18}H_{18}AuF_6I_2N_6P$ |
| Formula mass | 820.14 | 914.12 |
| Crystal system | monoclinic | monoclinic |
| Space group | *C*2/*c* | *C*2/*c* |
| *a* [Å] | 14.4535(5) | 15.5763(4) |
| *b* [Å] | 6.8128(2) | 6.9467(2) |
| *c* [Å] | 24.7857(9) | 23.4835(6) |
| *α* [°] | 90 | 90 |
| *β* [°] | 103.121(2) | 103.1720(10) |
| *γ* [°] | 90 | 90 |
| *V* [Å$^3$] | 2376.90(14) | 2474.15(11) |
| *Z* | 4 | 4 |
| Temperature [K] | 100(2) | 100(2) |
| $R_1$ | 0.0386 | 0.0227 |
| $wR_2$ [$I>2\sigma(I)$] | 0.0670 | 0.0444 |

## Acknowledgments

This work was supported by the National Science Foundation (CHE-0549902). The authors wish to acknowledge Prof. Jineun Kim from Gyeongsang National University and Dr. Adam L. Moore for their useful discussions regarding this work.

[1] M. J. Katz, K. Sakai, D. B. Leznoff, *Chem. Soc. Rev.* **2008**, *37*, 1884.
[2] J. Vicente, P. González-Herrero, Y. García-Sánchez, D. Bautista, *Inorg. Chem.* **2008**, *47*, 10662.
[3] E. J. Fernandez, M. C. Gimeno, A. Laguna, J. M. López-de-Luzuriaga, M. Monge, P. Pyykkö, D. Sundholm, *J. Am. Chem. Soc.* **2000**, *122*, 7287 and the references therein.
[4] H. Schmidbaur, A. Schier, *Chem. Soc. Rev.* **2008**, *37*, 1931.
[5] a) H. Schmidbaur, *Gold Bull.* **1990**, *23*, 11; b) H. Schmidbaur, *Chem. Soc. Rev.* **1995**, *24*, 391; c) A. Grohmann, H. Schmidbaur, in *Comprehensive Organometallic Chemistry II* (Eds.: E. W. Abel, F. G. A. Stone, G. Wilkinson), Pergamon, Oxford, **1995**, vol. 3, chapter 1; d) H. Schmidbaur, *Gold: Progress in Chemistry, Biochemistry and Technology*, Wiley, New York, **1999**; e) P. Pyykkö, *Angew. Chem. Int. Ed.* **2004**, *43*, 4412.
[6] R. J. Puddephatt, *Chem. Soc. Rev.* **2008**, *37*, 2012.
[7] a) E. J. Fernandez, A. Laguna, J. M. López-de-Luzuriaga, *Dalton Trans.* **2007**, 1969; b) E. J. Fernandez, A. Laguna, J. M. López-de-Luzuriaga, M. Monge, P. Pyykkö, N. Runeberg, *Eur. J. Inorg. Chem.* **2002**, 750; c) V. J. Catalano, S. J. Horner, *Inorg. Chem.* **2003**, *42*, 8430; d) M. E. Olmos, A. Schier, H. Schmidbaur, *Z. Naturforsch., Teil B* **1997**, *52*, 203.
[8] a) J. Vicente, M.-T. Chicote, M.-C. Lagunas, P. G. Jones, *J. Chem. Soc., Chem. Commun.* **1991**, 1730; b) A. Burini, R. Bravi, J. P. Fackler Jr, R. Galassi, T. A. Grant, M. A. Omary, B. R. Pietroni, R. J. Staples, *Inorg. Chem.* **2000**, *39*, 3158; c) O. M. Abu-Salah, *J. Organomet. Chem.* **1990**, *387*, 123; d) C. K. Lee, K. M. Lee, I. J. B. Lin, *Organometallics* **2002**, *21*, 10; e) O. Schuster, U. Monkowius, H. Schmidbaur, R. Shyama Ray, S. Krüger, N. Rösch, *Organometallics* **2006**, *25*, 1004; f) Q.-H. Wei, G.-Q. Yin, L.-Y. Zhang, Z.-N. Chen, *Organometallics* **2006**, *25*, 4941.
[9] P. Pyykkö, M. Straka, *Phys. Chem. Chem. Phys.* **2000**, *2*, 2489.
[10] a) F. Mendizabal, P. Pyykkö, N. Runeberg, *Chem. Phys. Lett.* **2003**, *370*, 733; b) N. Runeberg, M. Schütz, H.-J. Werner, *J. Chem. Phys.* **1999**, *110*, 7210.
[11] P. Pyykkö, F. Mendizabal, *Chem. Eur. J.* **1997**, *3*, 1458.
[12] P. Pyykkö, *Chem. Soc. Rev.* **2008**, *37*, 1967.
[13] M. Bardají, A. Laguna, *Eur. J. Inorg. Chem.* **2003**, 3069.
[14] J. P. Fackler Jr, *Inorg. Chem.* **2002**, *41*, 6959.
[15] a) V. J. Catalano, M. A. Malwitz, *Inorg. Chem.* **2003**, *42*, 5483; b) V. J. Catalano, A. O. Etogo, *J. Organomet. Chem.* **2005**, *690*, 6041; c) V. J. Catalano, A. O. Etogo, *Inorg. Chem.* **2007**, *46*, 5608.
[16] V. J. Catalano, M. A. Malwitz, A. O. Etogo, *Inorg. Chem.* **2004**, *43*, 5714.
[17] *March's Advanced Organic Chemistry* (Eds.: M. B. Smith, J. March), 5th ed., John Wiley & Sons, New York, **2001**.
[18] E. J. Fernandez, A. Laguna, M. E. Olmos, *Coord. Chem. Rev.* **2008**, *252*, 1630.
[19] R. Usón, A. Laguna, M. Laguna, P. G. Jones, G. M. Sheldrick, *J. Chem. Soc., Chem. Commun.* **1981**, 1087.
[20] R. Usón, A. Laguna, M. Laguna, B. R. Manzano, P. G. Jones, G. M. Sheldrick, *J. Chem. Soc., Dalton Trans.* **1984**, 285.
[21] E. J. Fernandez, P. G. Jones, A. Laguna, J. M. López-de-Luzuriaga, M. Monge, M. E. Olmos, R. C. Puelles, *Organometallics* **2007**, *26*, 5931.
[22] E. J. Fernandez, P. G. Jones, A. Laguna, J. M. López-de-Luzuriaga, M. Montiel, M. E. Olmos, J. Pérez, R. C. Puelles, *Organometallics* **2006**, *25*, 4307.
[23] E. J. Fernandez, A. Laguna, J. M. López-de-Luzuriaga, M. Monge, M. Montiel, M. E. Olmos, M. Rodríguez-Castillo, *Organometallics* **2006**, *25*, 3639.
[24] J. C. C. Chen, I. J. B. Lin, *Organometallics* **2000**, *19*, 5113.
[25] S. Gründermann, A. Kovacevic, M. Albrecht, J. W. Faller, R. H. Crabtree, *J. Am. Chem. Soc.* **2002**, *124*, 10473.
[26] X.-Y. Liu, H.-L. Zhu, *Synth. React. Inorg. Met.-Org. Nano-Met. Chem.* **2005**, *35*, 325.
[27] R. Usón, A. Laguna, M. Laguna, *Inorg. Synth.* **1989**, *26*, 85.
[28] G. M. Sheldrick, *SHELXTL, Structure Determination Software Suite*, version 6.10, Bruker AXS, Madison WI, **2001**.

Received: December 15, 2008
Published Online: March 12, 2009

  